# Buckling and Failure of Compression-loaded Composite Laminated Shells with Cutouts

Mark W. Hilburger[*]

*NASA Langley Research Center, Hampton Virginia 23681-2199*

**Results from a numerical and experimental study that illustrate the effects of laminate orthotropy on the buckling and failure response of compression-loaded composite cylindrical shells with a cutout are presented. The effects of orthotropy on the overall response of compression-loaded shells is described. In general, preliminary numerical results appear to accurately predict the buckling and failure characteristics of the shell considered herein. In particular, some of the shells exhibit stable post-local-buckling behavior accompanied by interlaminar material failures near the free edges of the cutout. In contrast another shell with a different laminate stacking sequence appears to exhibit catastrophic interlaminar material failure at the onset of local buckling near the cutout and this behavior correlates well with corresponding experimental results.**

## I.    Introduction

Thin-walled shell structures are a fundamental component found in aircraft, spacecraft, and launch vehicles. In many applications, these structural components contain cutouts or openings that serve as doors, windows, or access ports, or are used to reduce weight. Often, some type of reinforcement is used around a cutout to eliminate local deformations and stress concentrations that can cause local buckling or premature material failures. Thus, it is important to understand how a cutout affects the baseline performance of a shell structure without a cutout, how loads are redistributed around the cutout, and how the shell can be tailored to enhance performance and reduce weight. In addition, it is important to understand performance enhancements that can be obtained by using lightweight fiber-reinforced composite materials. Furthermore, these structures usually experience compression loads during vehicle operation and, as a result, their buckling response and material failure characteristics must be understood and accurately predicted in order to develop efficient, safe designs.

Many numerical and experimental studies of the buckling behavior of cylindrical shells have been conducted since the early 1900s. It took nearly 100 years to reach the point where robust, high-fidelity analysis tools and measurement technologies were available that could be used to conduct test-analysis correlations that include the effects of initial geometric, material, and manufacturing imperfections and the effects of load introduction and support conditions. Two noteworthy studies conducted at the NASA Langley Research Center that document these advanced capabilities are given in Refs. 1 and 2. It is worth pointing out that these two studies show that differences as small as 5% between corresponding analytical and experimental results can be obtained for buckling and postbuckling of compression-loaded, laminated-composite, circular cylindrical shells. This small difference is on the same order as the error that inherently exists in the use of nominal material properties. Thus, technology and physical insight now exists that can be used to develop greatly improved buckling design criteria, such as that presented in Ref. 3. An important part of such an effort would, of course, need to include the effects of cutouts and material failures on the structural performance.

In contrast to the body of work that exists for complete cylindrical shells and curved panels, studies that address the effects of a cutout on the buckling performance of cylindrical shells didn't appear until 1968.[4] Since 1968, only about 20 studies have appeared that address the effects of unreinforced cutouts that focus on the buckling behavior of compression-loaded isotropic and laminated-composite circular cylindrical shells and curved panels.[5-25] Some of the general lessons learned from these studies are as follows. The presence of a cutout in an isotropic circular cylindrical shell can cause a localized response to occur near the cutout when the shell is loaded. This localized response typically consists of large out-of-plane deformations, large magnitude stress concentrations, and rapidly varying stress gradients near the cutout. In a compression-loaded circular cylindrical shell, the cutout may cause a local buckling response to occur in the shell, near the cutout, at applied loads lower than the general instability load

---

[*] Senior Research Engineer, Structural Mechanics and Concepts Branch, Member, AIAA.

of the corresponding shell without a cutout. For some cases, this localized buckling is followed by a stable postbuckling response near the cutout, which is indicated by the fact that additional load can be applied to the shell before it exhibits overall collapse. However, other cases have shown that a local response in the shell can occur that causes a disturbance with enough kinetic energy to cause overall collapse to occur immediately after the local buckling occurs. Starnes[6, 11] suggested that the buckling of compression-loaded isotropic shells with a cutout is governed by the nondimensional geometric parameter $\tilde{a} = a^2/Rt$, where $a$ is the characteristic hole dimension and $R$ and $t$ are the shell radius and thickness, respectively. In addition, Starnes identified approximate ranges of the $\tilde{a}$ parameter that corresponded to the various behavioral trends described above.

For shallow, isotropic curved panels with a circular cutout and subjected to compression loads, it has been found that cutout size greatly affects the nonlinear behavior. For example, it has been shown that curved panels with relatively small cutouts exhibit a linear prebuckling state followed by an unstable global buckling response and those with somewhat larger cutouts exhibit a nonlinear prebuckling state followed by an unstable global buckling response. As the cutout size gets even larger, the panels exhibit a monotonically increasing load–end-shortening response. These results suggest that traditional linear bifurcation buckling analyses may misrepresent the physics of the response for a certain range of cutout sizes because of significant nonlinear behavior and should not be used for design.

Numerical and experimental studies of the response of compression-loaded, laminated-composite, circular cylindrical shells with unreinforced rectangular cutouts indicate similar response characteristics to those exhibited by corresponding isotropic shells. In addition, results have shown that localized regions of biaxial inplane compression stresses form in the shell near the cutout and that these regions of biaxial stresses couple with out-of-plane deformations of the shell wall, causing an unstable local buckling response to occur near the cutout. Hilburger[19, 20] has shown that the buckling of compression-loaded anisotropic shells with a cutout is governed by a stiffness-weighted nondimensional geometric parameter, similar to that proposed by Starnes, and a stiffness-weighted cutout aspect ratio. In addition, the initial local buckling and postbuckling response near the cutout are characterized by large-magnitude deformations and stresses that cause material failure. Furthermore, laminate orthotropy and initial shell imperfections have been shown to have a significant effect on the nonlinear response and buckling behavior of a laminated-composite, circular cylindrical shell with a cutout.

For shallow, laminated-composite, curved panels with a central circular cutout and subjected to compression loads indicate similar trends to those exhibited by the corresponding isotropic shells. However, whether the panel exhibits an unstable snap-through-type buckling response or a monotonically increasing load-end-shortening response, depends significantly on the panel orthotropy and anisotropy. Furthermore, numerical and experimental studies have identified cases where panels exhibited large-magnitude out-of-plane prebuckling deformations and buckling loads that exceeded the classical linear bifurcation buckling load. This behavior was contrary to previously known behavioral characteristics of compression-loaded shallow curved panels. It was determined that these response characteristics were caused by circumferential edge restraint on the loaded boundaries of the panels and indicated a high degree of boundary condition sensitivity.

Review of the literature cited herein indicates that the buckling response of a compression-loaded cylindrical shell with a cutout is becoming better understood. In addition, studies have been conducted that address numerical simulation of progressive failure in compression-loaded, laminated-composite, curved panels with a central circular cutout.[29, 30] However, validation results for predicting delamination type failures in postbuckled laminated composites are somewhat limited and additional validation is required for thin-walled buckling critical laminated composite shells. Therefore, the objective of the present study is to present numerical and experimental results that will illustrate typical buckling and failure response characteristics and trends for a compression-loaded, thin-walled, laminated-composite, circular cylindrical shell with a square cutout and several laminate stacking sequences. This shell configuration represents a generic example of a typical aerospace shell structure with a cutout subjected to a destabilizing load. To accomplish this objective, selected experimental and numerical results that illustrate the effects of laminate orthotropy on the buckling and failure response of compression-loaded shells with cutouts are presented. Results obtained from an advanced high-fidelity nonlinear analysis procedure that includes the effects of intralaminar and interlaminar is used in the study and offers the opportunity to provide insight into the effects of laminate orthotropy on the buckling and failure response of compression-loaded shell structures. In addition, preliminary results from a new, coupled nonlinear transient dynamic global collapse and progressive failure analysis method is presented. The results include load-shortening response curves, out-of-plane displacement response curves and displacement contours, and descriptions of the observed shell buckling and failure responses.

## II.   Test Specimens, Imperfection Measurements, and Tests

### A.  Test Specimens

Results from three test specimens that were fabricated and tested in a previous investigation are presented and are referred to herein as specimens C1-C3.  The specimens were fabricated from 12-in-wide, 0.005-in.-thick AS4/3502 unidirectional graphite-epoxy tape material.  The nominal unidirectional lamina properties of a typical 0.005-in.-thick ply with a fiber volume fraction of 0.62 are as follows: longitudinal modulus $E_1$ = 18.5 Msi, transverse modulus $E_2$ = 1.64 Msi, in-plane shear modulus $G_{12}$ = 0.87 Msi, and major Poisson's ratio $\nu_{12}$ = 0.30. The material was laid up by hand on a 15.75-in.-diameter mandrel and vacuum bagged and cured in an autoclave to form shells with different 8-ply shell-wall laminates.  These laminates include an axially stiff $[\mp 45/0_2]_s$ laminate, a quasi-isotropic $[\mp 45/0/90]_s$ laminate, and a circumferentially stiff $[\mp 45/90_2]_s$ laminate (a $0^o$ lamina ply and a $90^o$ lamina ply correspond to plies with fibers aligned along the length of the cylinder and around its circumference, respectively).  A 1.0-in by 1.0-in square cutout with 0.05-in-radius reentrant corners was machined in each cylinder at the shells mid-length.  The specimens had a nominal length $L$ equal to 16.0 in., a nominal radius $R$ equal to 8.0 in, and a nominal shell-wall thickness $t_{nom}$ equal to 0.04 in.  Both ends of the specimens were potted in an aluminum-filled epoxy resin to ensure that the ends of the specimen did not fail prematurely during the test.  The potting material extended approximately 1.0 inch along the length of the specimens at each end, resulting in a test section that is approximately 14.0-in. long.  The ends of the specimens were machined flat and parallel to a tolerance of ±0.001 inches to facilitate uniform load introduction during the tests.   A typical cylinder specimen with a centrally located square cutout is shown in Fig. 1.

### B.  Test Apparatus and Instrumentation

The specimens were instrumented with electrical-resistance strain gages.  In particular, sixteen back-to-back pairs of uniaxial strain gages were positioned around the perimeter of the cutout edge to characterize the rapidly varying strain gradients that develop during loading.  These gages were aligned tangent to the cutout edge at the four corners and at the mid-length of each of the four sides, as shown in Fig. 2.  In addition, far-field strain gages were positioned at several locations around the specimen to characterize the prebuckling load introduction into the specimen and load redistribution after local and global buckling occurs.

Direct-current differential transducers (DCDTs) were used to measure displacements.  In particular, several DCDTs were positioned in the interior of the specimen to measure radial displacements near the cutout, as shown in Fig. 2a.  In addition, three non-collinear DCDTs were positioned at three corners of the upper loading platen and used to measure the end-shortening displacement and the loading platen rotations, as shown in Fig. 1.

A shadow moiré interferometery technique was used to observe the shell-wall prebuckling, buckling, and postbuckling radial deformation patterns.  All data were recorded with a data acquisition system, and the moiré patterns were recorded photographically, on videotape, and with a high-speed digital video camera.  The high-speed digital video camera recorded images at a rate of 2000 Hz.

The specimens were loaded in compression with a 120-Kip hydraulic universal-testing machine by applying an end-shortening displacement to the shell ends (loading surfaces) of a specimen.  To control the load introduction into the specimen, the upper loading platen was aligned with the loading surface of the specimen before the test by adjusting leveling bolts in the corners of the upper loading platen until strains measured by selected far-field strain gages on the specimens indicated a uniform axial strain distribution around the circumference of the shell.  The specimens were loaded until global collapse and failure of the shells occurred.

### III.   Finite-element Models and Analysis Methods

### A.  Finite-Element Models

All the shells considered in this study were analyzed with the STAGS (Structural Analysis of General Shells) nonlinear shell analysis code. [31]  STAGS is a finite-element code designed for the static and dynamic analysis of general shells, and includes the effects of geometric and material nonuniformities and progressive interlaminar and intralaminar material failure.  The cylinders were modeled using the standard 410 quadrilateral elements from the STAGS element library.  This element is a flat facet-type element based on Kirchoff-Love thin-shell theory and the nonlinear Lagrangian strain tensor.   A more thorough explanation of model development and validation procedures

American Institute of Aeronautics and Astronautics

for high-fidelity modeling of compression-loaded composite laminated shells with and without cutouts is presented in Refs. 1 and 2.  The models also include the effects of progressive intralaminar and interlaminar material failures and preliminary results from these analyses are presented herein.   The progressive failure methodology is described next.

## B.  Progressive Failure Methodology

Intralaminar material failures were predicted by using the Hashin[32] failure criteria.   The progressive failure theory and implementation are discussed in Ref. 29 and 30.  Some relevant details are presented subsequently.
The intralaminar failure modes considered include matrix cracking, fiber-matrix shear failure, and fiber failure. To apply the failure criterion, the stress state is analyzed at each material point in the finite element model for a given solution step in the analysis.   If the failure criteria is met (i.e., if the Hashin failure index exceeds a value of 1.0) then it is assumed that the material at point has failed the material stiffnesses at that point are then degraded according to the Chang and Lessard degradation model.[33] Material allowables used in the present study for AS4/3502 material are as follows:  in-plane shear stress allowable $S_{12}$ = 25.5 ksi,  longitudinal tension and compression stress allowables $X_t$ = 200.0 ksi and $X_c$ = 180.0 ksi, respectively, and transverse tension and compression stress allowables $Y_t$ = 12.6 ksi and $Y_c$ = 24.6 ksi, respectively.

The initiation and progression of interlaminar, delamination failures are predicted by using a decohesion element that is positioned between composite laminae in potential delamination locations. A material-softening constitutive law developed by Goyal et al.[30] is used in the formulation of the decohesion element.  This constitutive law governs the initiation of a delamination and the subsequent delamination growth.   The initiation of a delamination is specified to occur when the maximum interfacial strength between plies is exceeded and subsequent propagation of the delamination occurs when the fracture energy release rate is exceeded.  The interfacial material failure properties used in the present study for AS4/3502 are as follows:  the critical energy release rates $G_{Ic}$ = 1.31 lb/in, and $G_{IIc}$ = $G_{IIIc}$ = 3.3 lb/in.  The maximum interfacial strengths $T_1^c$ = 9.0 ksi, and $T_2^c$, = $T_3^c$ = 10.5 ksi.   The decohesion element was implemented in the STAGS finite-element code as a user-defined element.

## IV. Results and Discussion

Numerically predicted and experimentally measured results for three compression-loaded composite cylindrical shells with cutouts are presented in this section.  The predicted results were obtained from finite-element analyses of geometrically and include the effects of intralaminar and interlaminar progressive failure.   First, experimentally measured results are presented for the three cylinders with different laminate stacking sequences to illustrate the typical buckling and failure response of the shells and provide a baseline for comparison with the numerically predicted results. The results include load-shortening response curves, load-strain response curves, and observed and predicted out-of-plane deformation patterns and material failures.  The values of axial load $P$, presented herein, are normalized with respect to the linear bifurcation buckling load of a geometrically perfect, quasi-isotropic cylinder without a cutout, $P_{cr}^o$ = 42,590 lb.  The end-shortening displacements are normalized by the specimen length $L$ = 16.0 in., respectively.

## A.  Experimental Results

Measured load–end-shortening response curves for the three cylinders with unreinforced cutouts, C1 ([∓45/0/90]$_s$), C2 ([∓45/0$_2$]$_s$), and C3 ([∓45/90$_2$]$_s$), considered in this study, are shown in Fig. 3.  Buckling loads are indicated by filled circles and global collapse loads are indicated by an **X**.  The cylinders exhibit a linear prebuckling load-shortening response up to buckling (note: the initial nonlinearity in the prebuckling response is attributed to the usual initial misalignment between the specimen and the loading platen).  Cylinders C1 and C2 exhibit a local buckling response at normalized load levels of 0.48 and 0.39, respectively.  The buckling response is characterized by localized, unstable dynamic buckling event in the cylinder and includes the formation of large-magnitude out-of-plane deformations and rapidly varying strains near the cutout.  It has been shown by Hilburger et al.[19, 20] that this local buckling response is caused by nonlinear coupling between the compressive in-plane biaxial stresses and the out-of-plane deformations that occur near the cutout.   A stable post-local-buckling response is exhibited by specimens C1 and C2 and additional load is carried by these shells until global collapse occurs at load levels of 0.52 and 0.41, respectively.  As loading continues in the post-local-buckling region of the response, these shells exhibit a slight reduction in the effective axial stiffness.  This reduction in axial stiffness, manifested by a change in slope of the response curves, is caused by increasingly large out-of-plane deformations that develop in the shell and cause a redistribution of load away from the cutout, there by reducing the effective load-carrying cross-section of the shell. The global collapse response is characterized by a significant reduction in axial load and the development of the

general instability deformation pattern.   Specimens C1 and C2 obtain stable post-collapse equilibrium at load levels of 0.32 and 0.23, respectively and can sustain additional loading until complete failure of the cylinders occurs due to significant accumulation of material failures in the shell wall.   In contrast, shell C3 exhibits an unstable local buckling response, at a load of  0.51, that caused a catastrophic failure of the specimen and, as a result, there was no residual post-buckling strength for this specimen.

The results in Fig. 3 and results in Reference 1 also indicate that the measured initial buckling load of specimens with a cutout are an average of 37.3% less than the measured buckling loads of the corresponding specimens without a cutout. However, there are no noticeable differences in the prebuckling stiffnesses of the specimens with the same laminate, regardless of whether there is a cutout or not.  Moreover, the measured post-buckling loads for specimens C1 and C2 after global collapse are 2.1 and 1.4%, respectively, greater than the corresponding buckling loads for the shells without cutouts and indicates that, in some cases, the cutout can have a relatively small effect on the post-buckling strength of these specimens.

Typical observed local buckling and global collapse out-of-plane deformation patterns for specimen C2 are shown Fig 4.   In general, the specimens exhibit small-magnitude prebuckling deformations.   During the local buckling response, the cylinders exhibit radial displacements at the corners of the cutout that range from -1.0 to +1.5 times the nominal shell-wall thickness.  After global collapse, the specimens exhibit displacements of approximately +2.0 to +3.0 times the shell-wall thickness.  The local buckling deformation response consists of large ellipse-like buckles on either side of the cutout and are aligned in a helical or skew direction (see Fig. 4a)  After additional load is applied, the specimens collapse into a general instability buckling pattern in which the local buckles near the cutout increase in size and magnitude, and additional buckles develop around the circumference of the specimen (see Fig. 4b).

Typical measured strain results for specimens C1, C2, and C3 are shown in Fig. 5.  The figure includes data from three axially aligned back-to-back strain gage pairs located at the right edge of the cutout in specimens C1-C3.  The solid and dashed lines denote measured strain data from gages located on the outer shell-wall surface and the inner shell-wall surface, respectively.  In general, the results indicate that specimens C1 and C2 exhibit some local bending during the prebuckling response, as indicate by the divergence of the back-to-back strain gage curves, and have maximum strains that approach 0.6% strain.   The strains near the cutout in specimens C1 and C2 increase significantly when local buckling and global collapse occur and can exceed 2.0% strain.   Once local buckling occurs, these large-magnitude bending strains near the cutout activate an interlaminar shear failure mechanism in specimens C1 and C2 as shown in Fig. 6 for specimen C1.  The local interlaminar shear failures that developed in specimens C1 and C2 typically propagate approximately 0.5 in. beyond the free edge of the cutout around the circumference of the shell.   In contrast, specimen C3 exhibits significant bending from the onset of loading and these large-magnitude bending strains activate an interlaminar shear failure mechanism prior to buckling.   The initial local failures that occur near the cutout in shell C3 propagated around the circumference of the specimen very rapidly and, as a result, this specimen had no post-buckling strength as shown in Fig 7.

## B.  Predicted Results

Predicted results were obtained for the three shell specimens, and include load–end-shortening response curves; pre-buckling, buckling, and post-buckling deformations; and selected results that illustrate the progressive interlaminar and intralaminar failure response of these shells.

Predicted load—end-shortening response curves for shells C1 through C3 are presented in Fig.  8.   Two predictions were obtained for each shell and include the effects of intralaminar or interlaminar (delamination) progressive failures in the analyses, denoted by the suffixes –PFA and –DELAM, respectively.  The local buckling events are marked with a filled circle symbols and global collapse or failure is marked with an **X**.  The results indicate that all the shells exhibit lower local buckling loads when including the effects of the interlaminar failures.  Shells C1 and C2 exhibit additional post-local-buckling load carrying capability until global collapse occurs as indicate by the X symbol and the sudden reduction in the axial load predicted by using the transient analysis capability in the STAGS finitie-element analysis code.  No significant growth in the damage zones occur during the initial global collapse event.  In contrast, shell C3 exhibits a local buckling event that couples with local interlaminar failures near the free edge of the cutout to cause the sudden failure of the shell.  This sudden failure of the shell is indicated by the rapid reduction in axial load and the significant propagation of the interlaminar failures around the circumference of the shell.

Typical predicted intralaminar and interlaminar material failures incipient to local buckling and global collapse for shell C1 are shown in Figs. 9a through 9d.  The results indicate some intralaminar failures in the upper and lower right corners of the cutout in the form of matrix tension failures and fiber compression failures. However, the analysis also predicts the initiation and propagation of interlaminar shear-type failures near the free-edge of the

American Institute of Aeronautics and Astronautics

cutout (see Figs 9c and 9d). The location and the extent of the damage in the shell appears to agree well with the observed damage shown in Fig. 6. Similar failure predictions were obtained for shell C2 and C3 and results for the circumferentially-stiff shell C3 are shown in Fig. 10. Predicted delamination-type failures in shell C2 are less pronounced than those predicted for shell C1 and agree well with the observed failure response in the shell. Preliminary failure predictions obtained for shell C3 indicate an increased potential for the initiation of interlaminar failures at the edges of the cutout and the rapid propagation of these delaminations around the circumference of the shell, as observed in the test. This increased potential for interlaminar shear failures is due to relatively large-magnitude bending strains (> 1% strain) and deformations near the cutout, as compared to the strains exhibited by shells C1 and C2. In addition, it is well established that delamination-type failures will initiate and propagate more easily in a structure where the lamina fibers are oriented parallel to the direction of propagation.

It should be noted that, at the time this paper was written, the final transient collapse and or failure predictions for all three shells were only partially complete and that the results and conclusions presented herein are based on response trends identified in the initial transient analysis results.

## V.    Concluding Remarks

Results from a numerical and experimental study of the response of compression-loaded, laminated-composite, cylindrical shells with either reinforced or unreinforced cutouts have been presented. The numerical results were obtained by using high-fidelity nonlinear finite-element analyses. The analysis accounted for the effects of intralaminar and interlaminar material failures. The results identify some of the effects of shell-wall orthotropy on the buckling and failure response of the shells. For the quasi-isotropic shell and the axially-stiff shell considered in the present study, the local buckling response near the cutout in the shell results in a stable post-local-buckling response and is accompanied by local interlaminar material failures near the cutout and additional load can be applied to the shell before it undergoes global collapse. In contrast, the local response near the cutout in the circumferentially-stiff shell causes a significant increase in the accumulation of interlaminar failures. Furthermore, preliminary results indicate that these interlaminar failures continue to accumulate throughout the transient collapse response and lead to the overall failure of the shell.

The selected results presented herein suggest that tailoring the laminate orthotropy, in a compression-loaded shell can result in significant increases in the buckling load of the shell, and can reduce the local strains, and damage accumulation near the cutout. The robust validated high-fidelity nonlinear analysis procedure used in this study offers the opportunity to provide insight into various laminate orthotropies on the buckling and failure response of compression-loaded shell structures. Moreover, results from such a high-fidelity analysis procedure can improve some of the engineering approximations and methods that are used in the design of composite shell structures with cutouts.

## References

1. Starnes, J. H., Jr., Hilburger, M. W., and Nemeth, M. P., "The Effects of Initial Imperfections on the Buckling of Composite Shells," *Composite Structures: Theory and Practice*, ASTM STP 1383, P. Grant and C. Q. Rousseau, Eds., American Society for Testing and Materials, 2000, pp. 529-550.

2. Hilburger, M. H., and Starnes, J. H., Jr., "Effects of Imperfections on the Buckling Response of Compression-loaded Composite Shells," International Journal of Non-linear Mechanics, Vol. 37, 2002, pp. 623-643.

3. Hilburger, M. W., and Nemeth, M. P., and Starnes, J. H., Jr., "Shell Buckling Design Criteria Based on Manufacturing Imperfection Signatures," NASA/TM-2004-212659, May, 2004.

4. Tennyson, R. C., "The Effects of Unreinforced Circular Cutouts on the Buckling of Circular Cylindrical Shells," *Journal of Engineering for Industry*, Transactions of the American Society of Mechanical Engineers, Vol. 90, November 1968, pp. 541-546.

5. Brogan, F. A. and Almroth, B. O., "Buckling of Cylinders with Cutouts," *AIAA Journal*, Vol. 8, No. 2, February 1970, pp. 236-240.

6. Starnes, J. H., Jr., "The Effect of a Circular Hole on the Buckling of Cylindrical Shells," Ph. D. Dissertation, California Institute of Technology, Pasadena, California, 1970.

7. Jenkins, W. C., "Buckling of Cylinders with Cutouts under Combined Loading," MDC Report G2476, October 1971, McDonnell-Douglas Astronautics Co.

8. Almroth, B. O. and Holmes, A. M. C., "Buckling of Shells with Cutouts, Experiment and Analysis," *International Journal of Solids and Structures*, Vol. 8, 1972, pp. 1057-1071.

9. Starnes, J. H., Jr., "Effect of a Slot on the Buckling Load of a Cylindrical Shell with a Circular Cutout, " *AIAA Journal*, Vol. 10, No. 2, February 1972, pp. 227-229.

10. Almroth, B. O., Brogan, F. A., and Marlowe, M. B., "Stability Analysis of Cylinders with Circular Cutouts," *AIAA Journal*, Vol. 11, No. 11, 1973, pp. 1582-1584.

11. Starnes, J. H., Jr., "The Effects of Cutouts on the Buckling of Thin Shells," *Thin-Shell Structures: Theory, Experiment, and Design*, edited by Y. C. Fung and E. E. Sechler, Prentice-Hall, Inc., Englewood Cliffs, New Jersey, 1974, pp. 289-304.

12. Almroth, B. O., Meller, E, and Brogan, F. A., "Computer Solutions for Static and Dynamic Buckling of Shells," *Buckling of Structures*, edited by B. Budiansky, IUTAM Symposium, Cambridge, Massachusetts, 1974, pp. 52-66.

13. Toda, S, "Buckling of Cylinders with Cutouts Under Axial Compression," *Experimental Mechanics*, Vol. 3, 1983, pp. 414-417.

14. Janisse, T. C. and Palazotto, A. N., "Collapse Analysis of Composite Panels With Cutouts," Proceedings of the AIAA/ASME/ASCE/AHS 24th Structures, Structural Dynamics, and Materials Conference, AIAA paper 83-0875, 1983.

15. Knight, N. F. and Starnes, J. H., Jr., "Postbuckling Behavior of Selected Graphite-Epoxy Cylindrical Panel Loaded in Compression," Proceedings of the AIAA/ASME/ASCE/AHS 27th Structures, Structural Dynamics, and Materials Conference, AIAA paper 86-0881-CP, 1986.

16. Knight, N. F. and Starnes, J. H., Jr., "Postbuckling Behavior of Axially Compressed Graphite-Epoxy Cylindrical Panels with Circular Holes," Proceedings of the 1984 ASME Joint Pressure Vessels and Piping/Applied Mechanics Conference, 1984.

17. Lee, C. E. and Palazotto, A. N., "Nonlinear Collapse Analysis of Composite Cylindrical Panels With Small Cutouts or Notches," Proceedings of the AIAA/ASME/ASCE/AHS 25th Structures, Structural Dynamics, and Materials Conference, AIAA paper 84-0889, 1984.

18. Madenci, E. and Barut, A., "Pre- and Postbuckling Response of Curved, Thin, Composite Panels with Cutouts Under Compression, *International Journal for Numerical Methods in Engineering*, Vol. 37, 1994, pp. 1499-1510.

19. Hilburger, M. W., "Numerical and Experimental Study of the Compression Response of Composite Cylindrical Shells with Cutouts," Ph. D. Dissertation, University of Michigan, Ann Arbor, Michigan, 1998.

20. Hilburger, M. W., Waas, A. M., and Starnes, J. H., Jr., "Response of Composite Shells with Cutouts Subjected to Internal Pressure and Compression Loads," *AIAA Journal*, Vol. 32, No. 2, 1999, pp. 232-237.

21. Hilburger, M. W., Starnes, J. H., Jr., and Waas, A. M. "A Numerical and Experimental Study of the Response of Selected Compression-loaded Composite Shells with Cutouts," Proceedings of the 39th AIAA/ASME/ASCE/AHS/ASC Structures, Structural Dynamics, and Materials Conference, Long Beach, CA, AIAA Paper No. 98-1768, 1998.

22. Jullien, J. F. and Limam, A., "Effects of Openings on the Buckling of Cylindrical Shells Subjected to Axial Compression, *Thin-Walled Structures*, Vol. 31, 1998, pp. 187-202.

22. Nemeth, M. P. and Starnes, J. H., Jr., "The NASA Monographs on Shell Stability Design Recommendations: A Review and Suggested Improvements, NASA/TP-1998-206290, January 1998.

23. Hilburger, M. W., Britt, V. O., and Nemeth, M. P., "Buckling Behavior of Compression-Loaded Quasi-Isotropic Curved Panels with a Circular Cutout, ," *International Journal of Solids and Structures*, Vol. 38, 2001, pp. 1495-1522.

24. Tafreshi, A., "Buckling and Post-buckling Analysis of Composite Cylindrical Shells with Cutouts Subjected to Internal Pressure and Axial Compression Loads," *International Journal of Pressure Vessels and Piping*, Vol. 79, 2002, pp. 351-359.

25. Madenci, E. and Barut, A., "The Influence of Geometric Irregularities on the Linear Buckling of Cylindrical Shells with an Elliptical Cutout," Proceedings of the 44th AIAA/ASME/ASCE/AHS/ASC Structures, Structural Dynamics, and Materials Conference, Norfolk, VA. AIAA Paper No. 2003-1929, 2003.

26. Cervantes, J. A. and Palazotto, A. N., "Cutout Reinforcement of Stiffened Cylindrical Shells," *Journal of Aircraft*, Vol. 16, No. 3, 1979, pp. 203-208.

27. Hilburger, M. W., and Starnes, J. H., Jr., "Bucking of Compression-loaded Composite Cylindrical Shells with Reinforced Cutouts," Proceedings of the AIAA/ASME/ASCE/AHS/ASC 43rd Structures, Structural Dynamics, and Materials Conference, Denver, CO. AIAA Paper No. 2002-1516, 2002.

28. Hilburger, M. W., and Starnes, J. H., Jr., "Bucking of Compression-loaded Composite Cylindrical Shells with Reinforced Cutouts," NASA/TM-2004-212656, September 2004.

29. Jaunky, N., Ambur, D. R., Davila, C. G., and Hilburger, M. W., "Progressive Failure Studies of Composite Panels with and without Cutouts," NASA/CR-2001-211223, September 2001.

30. Vinay, K. G., Jaunky, N., Johnson, E. R., and Ambur, D. R., "Intralaminar and Interlaminar Progressive Failure Analyses of Composite Panels with Circular Cutouts," Proceedings of the AIAA/ASME/ASCE/AHS/ASC 43rd Structures, Structural Dynamics, and Materials Conference, Denver, CO. AIAA Paper No. 2002-1745, 2002.

31. Rankin, C. C., Brogan, F. A., Loden, W. A., and Cabiness, H. D., "STAGS Users Manual, Version 5.0," Lockheed Martin Missiles & Space Co., Inc., Advance Technology Center, Report LMSC P032594, 2005.

32. Hashin, Z., "Failure Criteria for Unidirectional Fiber Composites," *Journal of Applied Mechanics*, 47, 1980, pp. 329-334.

33. Chang, F. K., and Lessard, L., "Damage Tolerance of Laminated Composites Containing an Open Hole and Subjected to Compressive Loadings: Part I – Analysis," *Journal of Composite Materials*, 25, 1991, pp. 2-43.
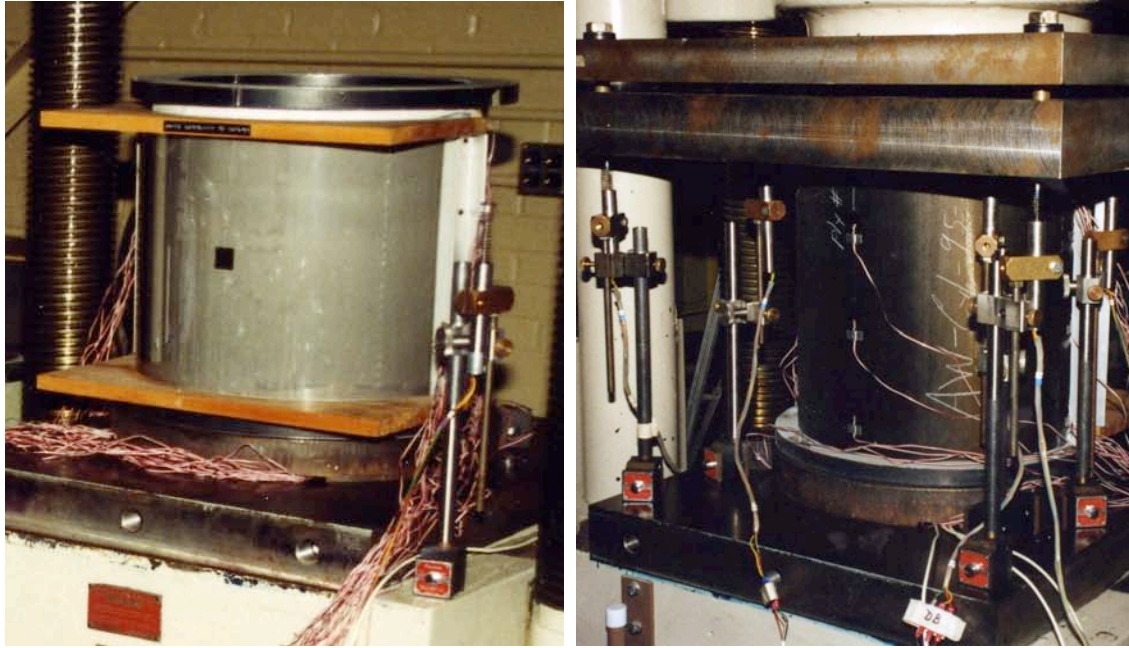
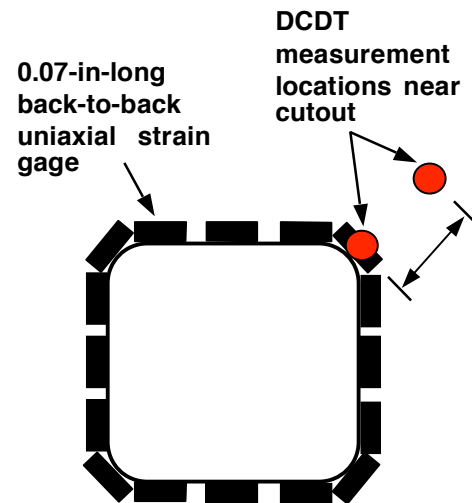a) Front view                                                b) Rear view

Fig. 1  Typical test set-up for a compression-loaded composite cylinder with a cutout.
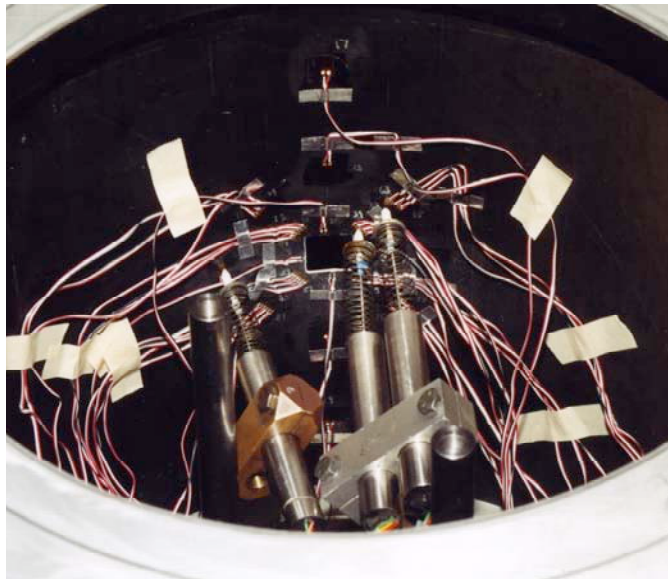


a) Internal strain gages and DCDTs                    b) Instrumentation pattern near cutout

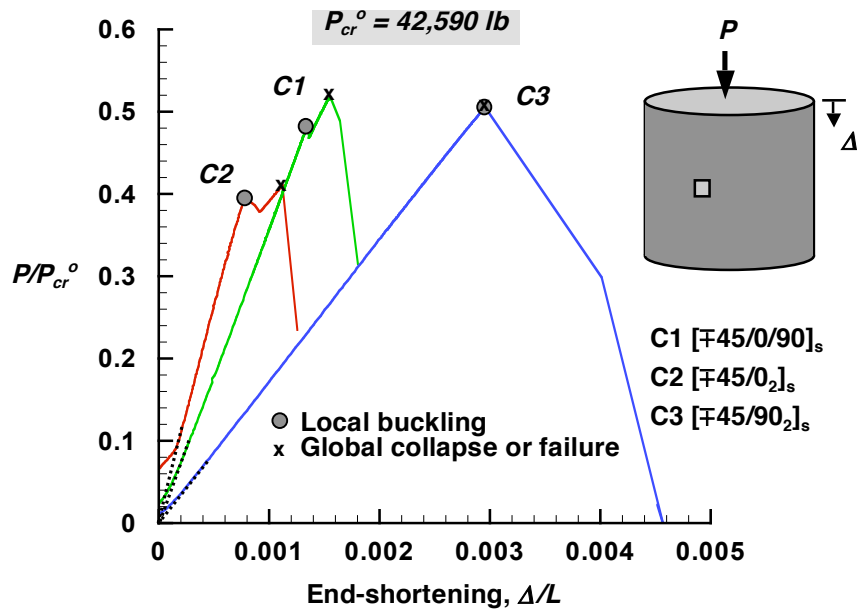Fig.  2  Typical DCDT and strain gage instrumentation near the cutout.

American Institute of Aeronautics and Astronautics

Fig. 3 Load-shortening response curves for compression-loaded composite cylinders with unreinforced 1-in. by 1-in. square-shaped cutouts ($P_{cr}^o$ = 42,590 lb is the linear bifurcation buckling load of the corresponding geometrically perfect quasi-isotropic shell without a cutout).
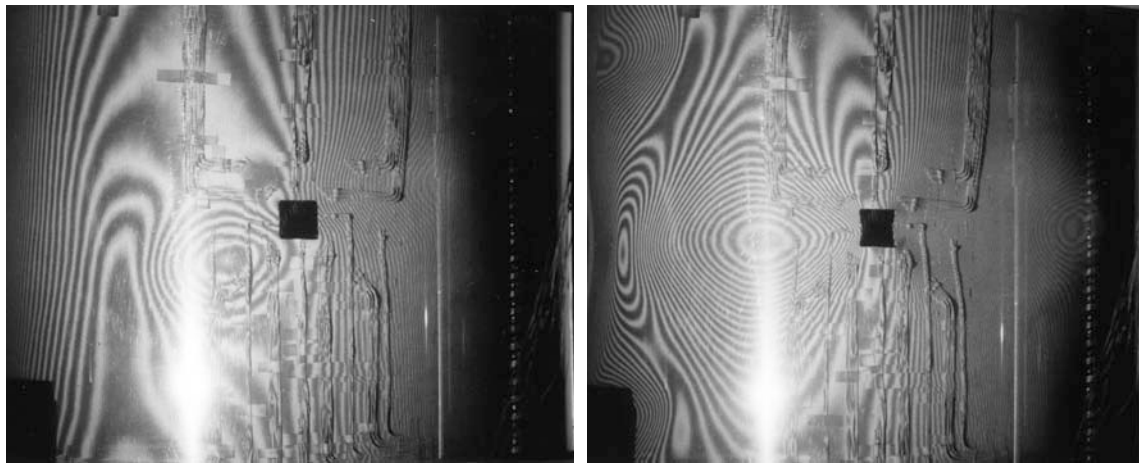


a) Local buckling moiré fringe pattern



b) Global collapse moiré fringe pattern

Fig. 4 Observed radial deformation patterns near a cutout for specimen C2.
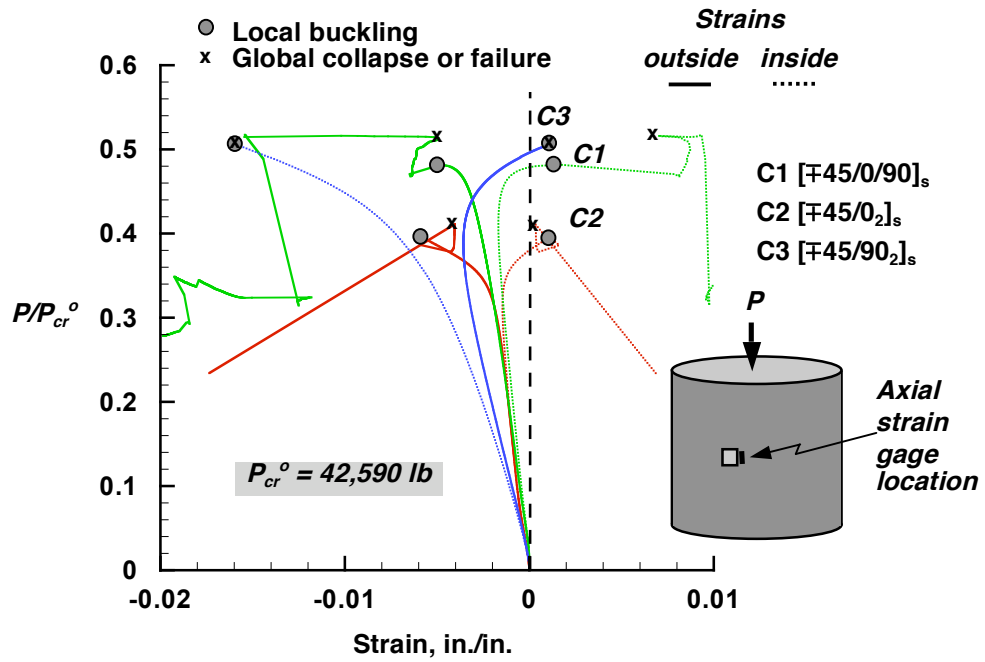
Fig. 5  Load-strain response near unreinforced 1-in. by 1-in. square-shaped cutouts in compression-loaded composite cylinders ($P_{cr}^o$ = 42,590 lb is the linear bifurcation buckling load of the corresponding geometrically perfect quasi-isotropic shell without a cutout).
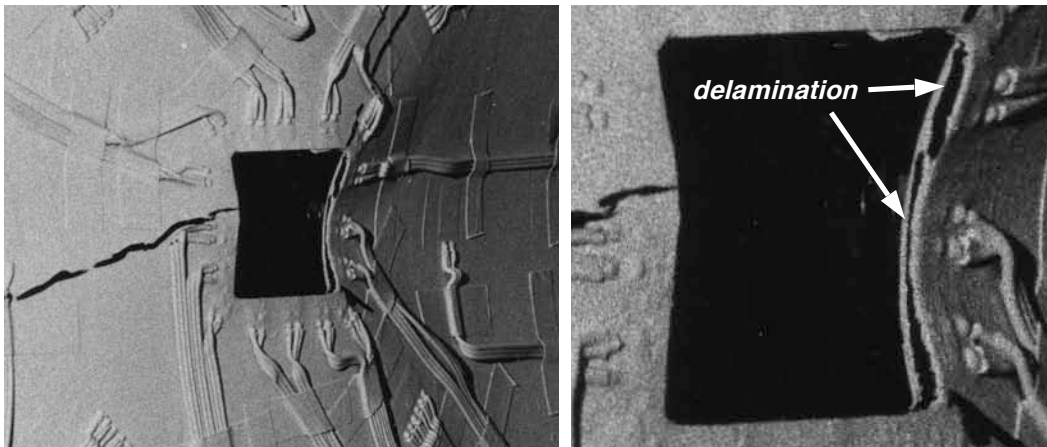


a) delamination at the right edge of the cutout          b) magnified view of cutout delamination

Fig. 6  Observed local delamination failures in specimen C1.
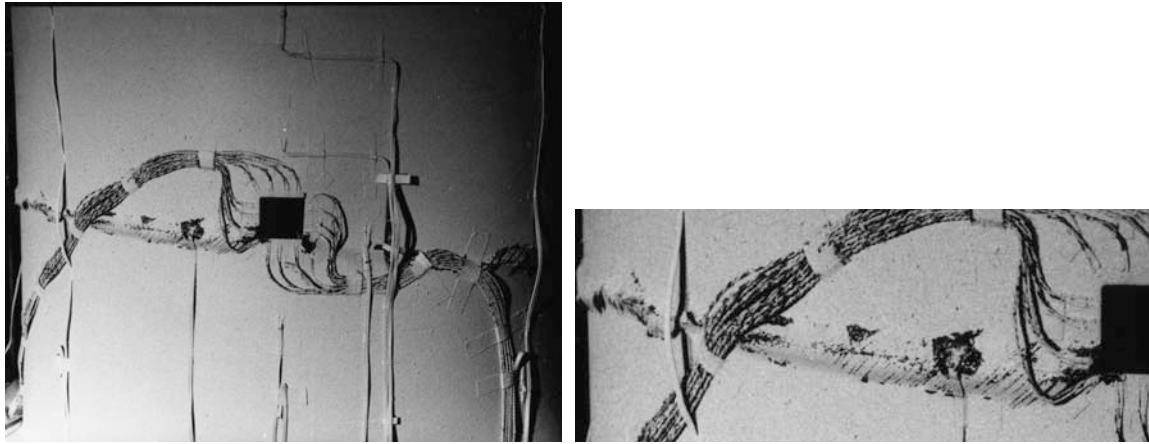
a) global view of failed specimen          b) magnified view of delamination on left side

Fig. 7  Observed catastrophic delamination failures in specimen C3.
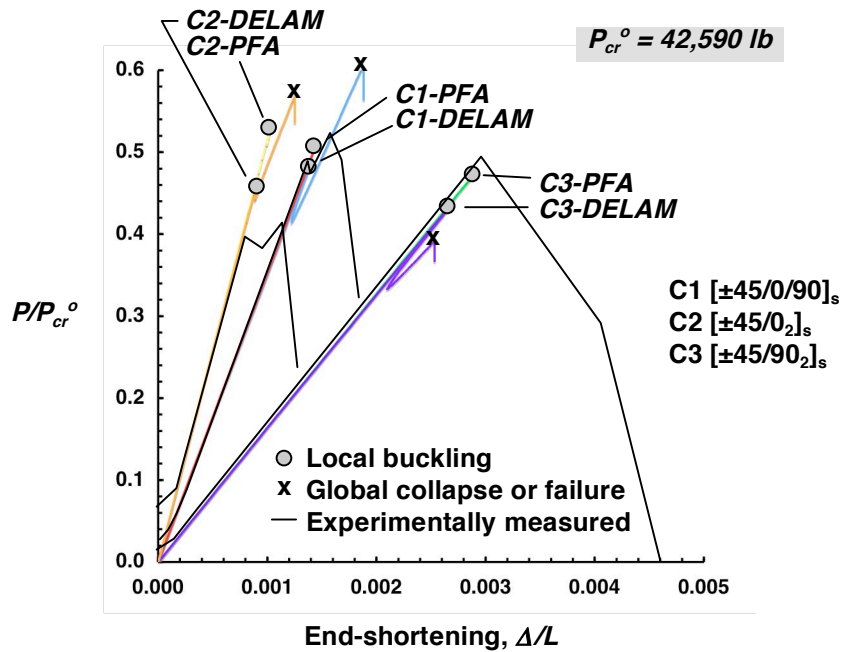


Fig. 8  Predicted load—end-shortening response curves for compression-loaded laminated composite cylinders and including the effects of interlaminar (DELAM) or intralaminar (PFA) progressive material failures. $P_{cr}^{o} = 42,590$ lb is the predicted linear bifurcation buckling load of the corresponding geometrically perfect quasi-isotropic shell without a cutout.
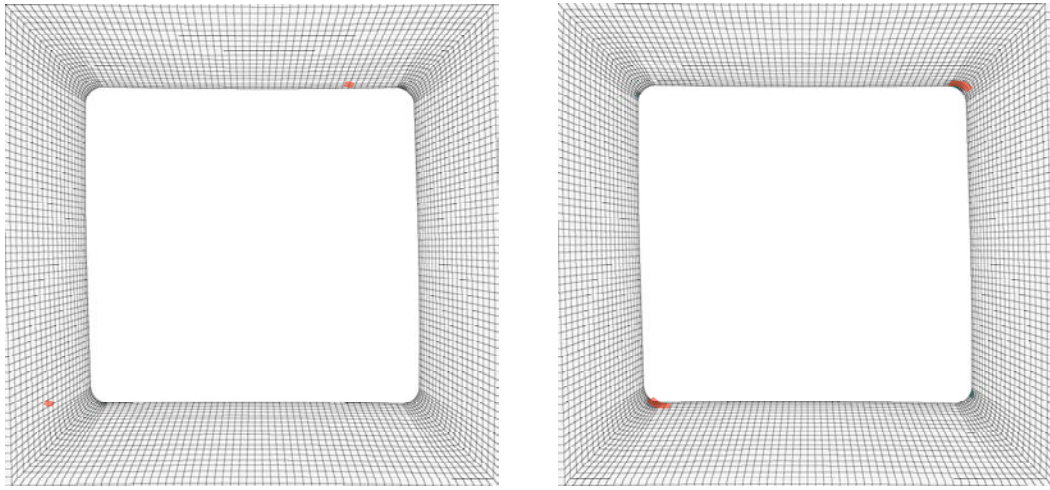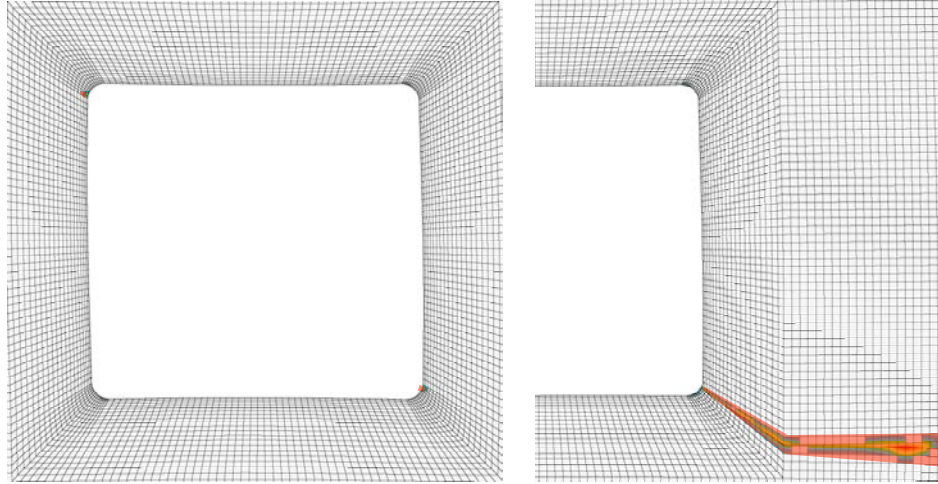
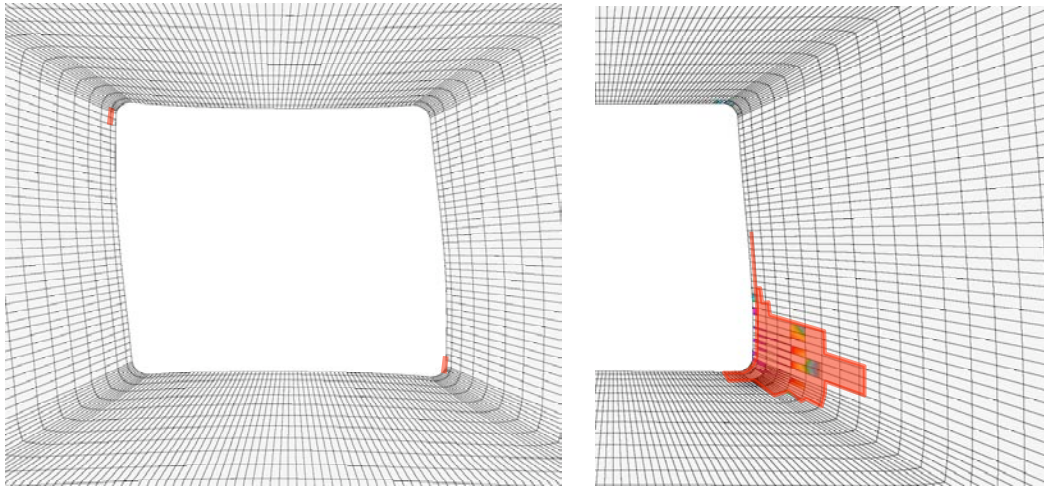a) Intralaminar failures
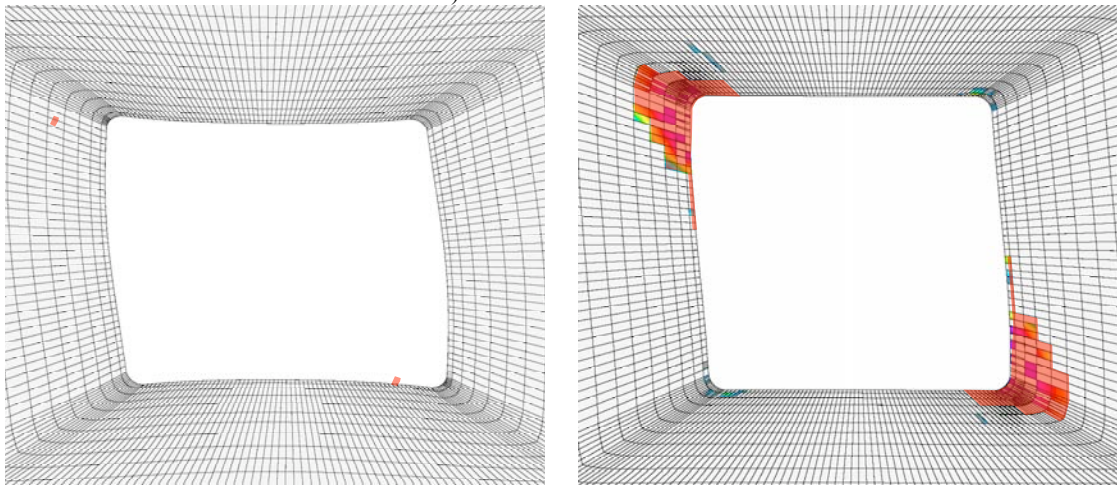


b) Interlaminar (delamination) failures

Fig. 9  Predicted local material failures for quasi-isotropic specimen C1 (extent of failures shaded in red for clarity).

a) Intralaminar failures



b) Interlaminar (delamination) failures

Fig. 10  Predicted local material failures for circumferentially-stiff specimen C3 (extent of failures shaded in red for clarity).